JACS
JOURNAL OF THE AMERICAN CHEMICAL SOCIETY

ARTICLE

pubs.acs.org/JACS

Spectroscopic and Microscopic Investigation of Gold Nanoparticle Formation: Ligand and Temperature Effects on Rate and Particle Size

Rajesh Sardar[†] and Jennifer S. Shumaker-Parry*

Department of Chemistry, University of Utah, 315 South 1400 East, RM 2020, Salt Lake City, Utah 84112, United States

Supporting Information

ABSTRACT: We report a spectroscopic and microscopic investigation of the synthesis of gold nanoparticles (AuNPs) with average sizes of less than 5 nm. The slow reduction and AuNP formation processes that occur by using 9-borabicyclo-[3.3.1]nonane (9-BBN) as a reducing agent enabled a time-dependent investigation based on standard UV−vis spectroscopy and transmission electron microscopy (TEM) analyses. This is in contrast to other borohydride-based syntheses of thiolate monolayer protected AuNPs which form particles very rapidly. We investigated the formation of 1-octadecanethiol (ODT) protected AuNPs with average diameters of 1.5−4.3 nm. By studying the progression of nanoparticle formation over time, we find that the nucleation rate and the growth time, which are interlinked with the amount of ODT and the temperature, influence the size and the size dispersion of the AuNPs. High-resolution TEM (HRTEM) analyses also suggest that the nanoparticles are highly single crystalline throughout the synthesis and appear to be formed by a diffusion-controlled Ostwald-ripening growth mechanism.

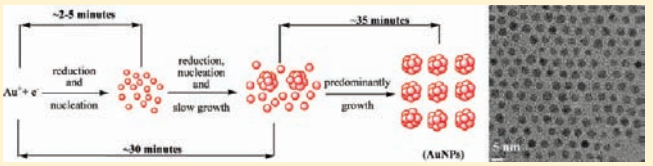

INTRODUCTION

Applications in electronic and optical detection systems,[1,2] device development,[3−5] therapeutics,[6] and catalysis[7,8] have made gold nanoparticles (AuNPs) the focus of much nanoscience research. The optical, electronic, and catalytic properties of metal nanoparticles are correlated with the physical characteristics of the particles, such as size[9−13] and shape[14−23] as well as the local dielectric environment.[24−27] In addition to the optical and electronic properties, the chemical properties of AuNPs are strongly related to the core size of the particles, and as the size of the particles decreases, the fraction of the atoms present on the vertex and edge sites increases in comparison to the terrace sites.[28] For example, the atoms in different sites on the nanoparticle surface substantially influence surface behavior including ligand place exchange reactions[29−31] as well as the electronic properties, such as the double-layer capacitance[32−41] and the anion-induced adsorption.[42−44] Because of the strong interrelationship, precise control of metal nanoparticle structural properties, such as size, surface chemistry, and even crystalline character, is a key goal for fundamental studies to better understand and control the optical, electronic, chemical, and electrochemical properties of AuNPs. Despite all of the synthetic work to produce metal nanoparticles, the extent of control of structural properties when particles are prepared in solution-based synthesis continues to be a challenge.[45−51]

The Brust two-phase synthesis and its various modifications are the most common approaches used to generate AuNPs with average diameters of 1−4 nm using $NaBH_4$ as a reducing agent.[52−61] In these synthetic methods strong stabilizing agents, such as alkyl or arylthiols, have been most commonly used to control the size of the nanoparticles. In these cases, the reduction usually reaches completion within a few hundred milliseconds after addition of the strong reducing agent $NaBH_4$ that typically is used. Other than $NaBH_4$, few other borohydride-based reducing agents have been used to synthesize stable, monodisperse AuNPs with diameters of <5.0 nm.[62,63] A key aspect of producing nanoparticles with a high degree of control of structural characteristics, such as particle size, size dispersion, shape, and crystallinity, is characterizing the nanoparticle formation process, including the role of changes in reaction parameters. Recently, mass spectrometry was used to investigate the growth of thiolate-protected AuNPs at various stages of particle formation.[64] Using mass spectrometry requires vigorous cleaning of the sample for every step of the analyses to remove unwanted or side products in order to achieve adequate resolution for data interpretation making this approach challenging. Another approach is to use real-time, in situ transmission electron microscopy (TEM) analysis with nanometer scale resolution, although this is quite challenging due to the fast rate of most nanoparticle formation processes. As an example, Alivisatos and co-workers used TEM to monitor the nucleation and the growth of platinum nanoparticles (PtNPs) in situ using a liquid cell.[65] In this case, the electron beam actually initiated the reduction reaction and was then used for imaging of the nanoparticle formation. The PtNP formation was quite rapid, making it difficult to obtain detailed information about the early nucleation and growth processes. However, the in situ TEM monitoring made it possible to at least observe the later growth stages and identify different growth mechanisms. Recognizing the challenges associated with these approaches, a much more ideal situation would be that more simple spectroscopic and microscopic methods could be used to

Received: September 10, 2010
Published: May 06, 2011

dx.doi.org/10.1021/ja107934h | J. Am. Chem. Soc. 2011, 133, 8179–8190

study the nanoparticle formation processes in a time-dependent manner. However, this typically is not feasible due to the fast rate of particle formation, especially for the most common synthetic methods used to produce metal particles with diameters of <5 nm.

We recently showed that the organo-borane reducing agent 9-borabicyclo[3.3.1]nonane (9-BBN) can be used for the synthesis of monodisperse metal nanoparticles with diameters of <5 nm. The mild reducing character of 9-BBN enabled the synthesis of AuNPs functionalized with a wide range of ω-functionalized ($HSC_{11}X$, X = −COOH, −OH, $-NH_2$, and $-N_3$) alkylthiols and phosphine ligands. We further demonstrated the versatility of 9-BBN as a reducing agent by the preparation of palladium, platinum, and silver nanoparticles.[66,67] Another consequence of using 9-BBN is that the nanoparticle formation process is rather slow compared to other borohydride-based syntheses. This is in contrast to the Brust two-phase process which uses $NaBH_4$ as a reducing agent and involves the very rapid formation of AuNPs. This is due to the enormous amount of hydride formed by the $NaBH_4$ during the reaction. The metal ions undergo very fast reduction in the presence of a high concentration of hydride, and the entire nanoparticle formation process takes only a few hundred milliseconds.[68,69] In contrast, 9-BBN-based synthesis of metal nanoparticles can take up to ~160 min depending on the reaction conditions.

Here we take advantage of the slow AuNP formation process induced by 9-BBN to study the growth process in a time-resolved manner using standard spectroscopic and microscopic techniques. We investigated AuNP formation based on reduction of Et_3PAuCl by 9-BBN using UV−vis absorption spectroscopy and TEM analyses. We investigated the role of the stabilizing agent concentration and the reaction temperature on the nucleation rate and growth time which ultimately control the final size and the size dispersion of the AuNPs. Time-dependent, high-resolution TEM (HRTEM) analysis provides evidence of a diffusion-controlled Ostwald-ripening growth mechanism, which leads to the generation of nanoparticles with a narrow size dispersion. To the best of our knowledge, this is the first example where the formation process of thiolated ligand protected AuNPs based on borohydride synthesis has been studied systematically by combining the simple approaches of UV−vis absorption spectroscopy and TEM analyses.

EXPERIMENTAL SECTION

Chemicals. Chloro(triethylphosphine) gold(I), 1-octadecanethiol (ODT), trioctylamine (TOA), and 9-BBN (0.5 M in THF) were purchased from Aldrich. HPLC grade toluene was obtained from Fisher Scientific. All chemicals and solvents were used as received without any purification. The glassware used in the synthesis was cleaned with aqua-regia (chemical warning: aqua-regia is very corrosive and should be handled with extreme care) and then rinsed with copious amounts of nanopure water and dried overnight prior to use. All reactions were carried out in air.

Spectroscopy and Microscopy Measurements. Absorption spectra (400−800 nm) were collected using a Perkin-Elmer Lambda 19 UV−vis/NIR spectrophotometer. TEM micrographs were obtained using a Tecnai-12 instrument operating at 100 KV. HRTEM images were collected using a JEOL 2010F-FAS instrument at 200 KV. Before TEM sample preparation, the sample was centrifuged at 4000 rpm for 10 min to remove any large aggregates present. From the centrifuged solution, one drop of reaction mixture was deposited on a 150-mesh Formvar-coated copper grid, and excess solution was removed by wicking with filter paper to avoid particle aggregation. The grid was then allowed to dry before being imaged. Particle size analysis was conducted by analyzing at least 200 particles in the TEM images using Scion Image Beta 4.02 software. In Scion Image, after setting the known distance and unit, the 'analyze particle' parameter was used to generate a table of particle diameters. This table was then exported into Microsoft Excel 2003 for statistical analysis. In a similar way, we calculated the interparticle spacing by analyzing a minimum of 150 interparticle spacings. Images with a 40 nm scale bar were used for particle spacing calculations, and the edge-to-edge distances of adjacent particles were taken into consideration.

Scheme 1. Synthesis of Alkylthiolate Protected AuNPs Synthesized Using 9-BBN as the Reducing Agent

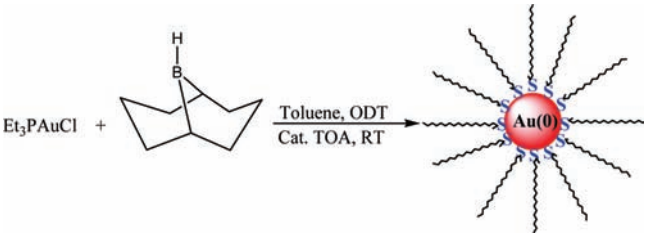

Synthesis of ODT Capped Gold Nanoparticles (AuNPs). In air at room temperature, 0.017 g (0.05 mmol) of Et_3PAuCl was dissolved in 100 mL of toluene. The solution was stirred for 5 min and then 0.17 g (0.5 mmol) of ODT was injected, and stirring was continued for another 30 min. At this point, 0.2 mL of 0.5 M 9-BBN in THF was added followed by immediate injection of 0.005 mL (0.01 mmol) of TOA. The color of the solution gradually changed from light purple to purple, and 65 min after the addition of 9-BBN, the color was reddish purple. The stirring was stopped, and the solution was centrifuged to remove any large aggregates. One drop of the centrifuged solution was deposited on a Formvar-coated copper grid and analyzed by TEM. Under identical molar amounts of gold salt and reducing agent, the reduction also was carried out in the presence of different amounts of ODT as described above. The toluene was then removed on a rotary evaporator. The black solid was suspended in 50 mL of ethanol and sonicated for 30 min. The solid was centrifuged out at 7000 rpm for 10 min. The sonication and centrifugation steps were performed three additional times. The solid was then dissolved in CH_2Cl_2, the solvent was removed using a rotary evaporator, and the solid was left under high vacuum for 2 h. The black solid was finally dissolved in CD_2Cl_2 and analyzed by ^1H NMR (see Supporting Information, Figure 1). The ^1H NMR data revealed no traces of unreacted ODT or 9-BBN. The presence of Et_3P from Et_3PAuCl also was not observed in the sample.

Synthesis of AuNPs at Different Temperatures. In the synthetic procedure, 0.017 g (0.05 mmol) of Et_3PAuCl was dissolved in 100 mL of toluene in air at room temperature. After the solution was stirred for 5 min, 0.17 mL (0.5 mmol) of ODT was injected, and stirring was continued for another 30 min. The solution was then adjusted to the stable temperature chosen for that particular synthesis. Next, 0.2 mL of 0.5 M 9-BBN in THF and 0.005 mL (0.01 mmol) of TOA were added to the reaction mixture. The AuNPs were synthesized at various solution temperatures from 25 to 70 °C. The reaction progress was monitored by UV−vis absorption spectroscopy, and as soon as a stable absorption λ_{max} was observed, the solution was removed from heat and allowed to cool to room temperature.

RESULTS AND DISCUSSION

Synthesis and Characterization of Thiolate-Stabilized AuNPs. At room temperature, 0.017 g (0.05 mmol) of Et_3PAuCl

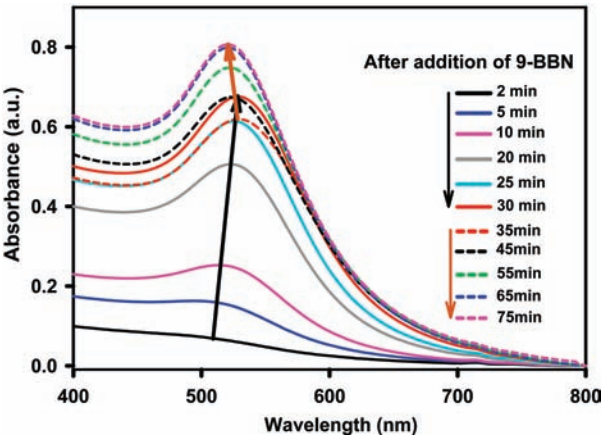

Figure 1. UV−vis absorption spectra of AuNPs at different time points of the synthesis after addition of 9-BBN.

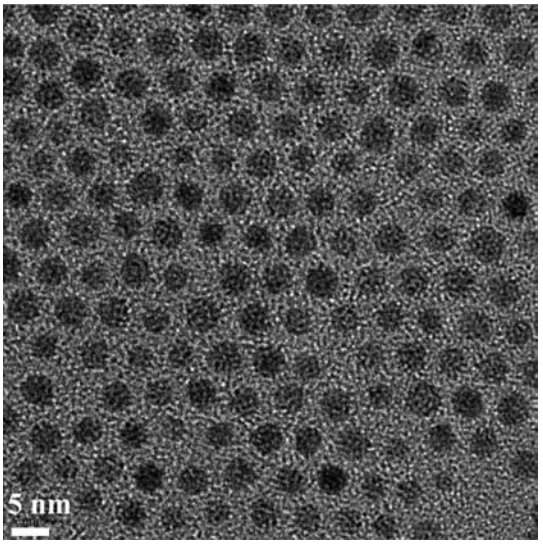

Figure 2. TEM image of AuNPs synthesized at room temperature using 9-BBN.

was dissolved in 100 mL of toluene in air, producing a colorless homogeneous solution. The solution was stirred for 5 min, and then 0.17 mL (0.5 mmol) of ODT was injected, and stirring was continued for another 30 min. At this point, 0.2 mL of 0.5 M 9-BBN in THF was added. Over time, the reaction mixture remained colorless even after 24 h of stirring. The solution displayed a featureless UV−vis absorption spectrum, and no nanoparticles were observed using TEM analysis, indicating the reduction reaction did not take place under these conditions.

To make the reduction reaction proceed, under similar reaction conditions and identical molar ratios of gold salt, thiol, and 9-BBN, a catalytic amount, 0.005 mL (0.01 mmol), of TOA was immediately injected after addition of 9-BBN (see Scheme 1). Within five minutes after addition of 9-BBN, the colorless solution gradually became light purple and then purple, and at the end of the reaction it was a reddish-purple color. The reddish-purple color of the solution is attributed to the localized surface plasmon resonance (LSPR) of AuNPs with a diameter greater than 2 nm present in the solution.[9] In the 9-BBN based production of gold nanoparticles, the tertiary amine TOA plays an important role because it is expected to polarize the B−H bond of 9-BBN and facilitate hydride liberation,[66] which eventually reduces the gold ions to gold atoms in the process of metal nanoparticle formation.

The progress of the reduction process was monitored by UV−vis absorption spectroscopy at different time intervals, see Figure 1. Approximately 2 min after addition of 9-BBN, the color of the solution was faint purple and displayed a featureless UV−vis spectrum. At 10 min, the purple-colored solution exhibited a LSPR peak (λ_{max}) at 513 nm. The LSPR peak red shifted and increased in amplitude for an additional 20 min, and at that point, the λ_{max} was 529 nm. At 35 min, the amplitude of the LSPR peak decreased, although the λ_{max} position remained unchanged. Beyond 35 min, after the decrease in amplitude, we observed a blue shift of the LSPR band compared to the LSPR λ_{max} at the 30-min time point. At later times, the LSPR peak continued to blue shift, and we also observed an increase in the peak amplitude. At 65 min, the solution exhibited a stable LSPR λ_{max} at 520 nm, and no further change in peak amplitude was observed. The observed LSPR changes are discussed in more detail below.

After a stable LSPR λ_{max} was observed at 65 min, the solution from the reaction was collected for TEM analysis. Figure 2 presents a representative TEM image of the product. The synthesis produces AuNPs which are nearly monodisperse in size with an average diameter of 3.3 ± 0.3 nm. In addition, the particles formed an ordered two-dimensional (2-D) array (see Figure 2). We observed that the 2-D arrangement of AuNPs did not extend across an extensive area of the TEM grid and that there were some void spaces in the assembly. This observation correlates with reports that when AuNPs are coated with long-chain alkylthiols, the formation of extended 2-D assemblies is rather poor[70] and could be attributed to an inhomogeneous coating of the thiols on the surfaces of the nanoparticles. Also, capillary forces would be expected to play an important role in the nanoparticle assembly, but the drying process was not controlled in the sample preparation. In fact, the large void spaces are likely due to the evaporation of the solvent after deposition of the sample solution on the TEM grid. Better control of solvent evaporation, as well as adhesion forces, may lead to more long-range order. Despite the lack of long-range order, the AuNP assembly appears to have quite uniform short-range order. We analyzed the short-range periodic arrangement of the nanoparticles and found a 2.2 ± 0.2 nm gap between adjacent particles. The predicted interparticle spacing ($2l$) based on assuming the particles are coated with a close-packed ligand shell was calculated using the previously reported formula, $l = 0.25 + 0.127n$, where n corresponds to the number of methylene ($-CH_2$) units in the carbon chain, and the value 0.25 was taken into consideration for the terminal methyl group and carbon−sulfur bond.[71] Based on this formula, we estimate an ODT chain length of 2.4 nm and an expected interparticle spacing (edge-to-edge) of 4.8 nm, which is twice the length of a single, extended ODT molecule. The experimental interparticle distance is 2.6 nm shorter than the calculated spacing. The shorter observed interparticle distance could be due to the ODT hydrocarbon chains attached to the AuNP surface not being fully extended or perhaps the ODT molecules from adjacent nanoparticles are interdigitated.[72] Either situation would result in an observed particle separation that is less than the theoretically calculated distance. Another contribution to the differences may be that the TEM analysis was performed on a 2-D plane of a

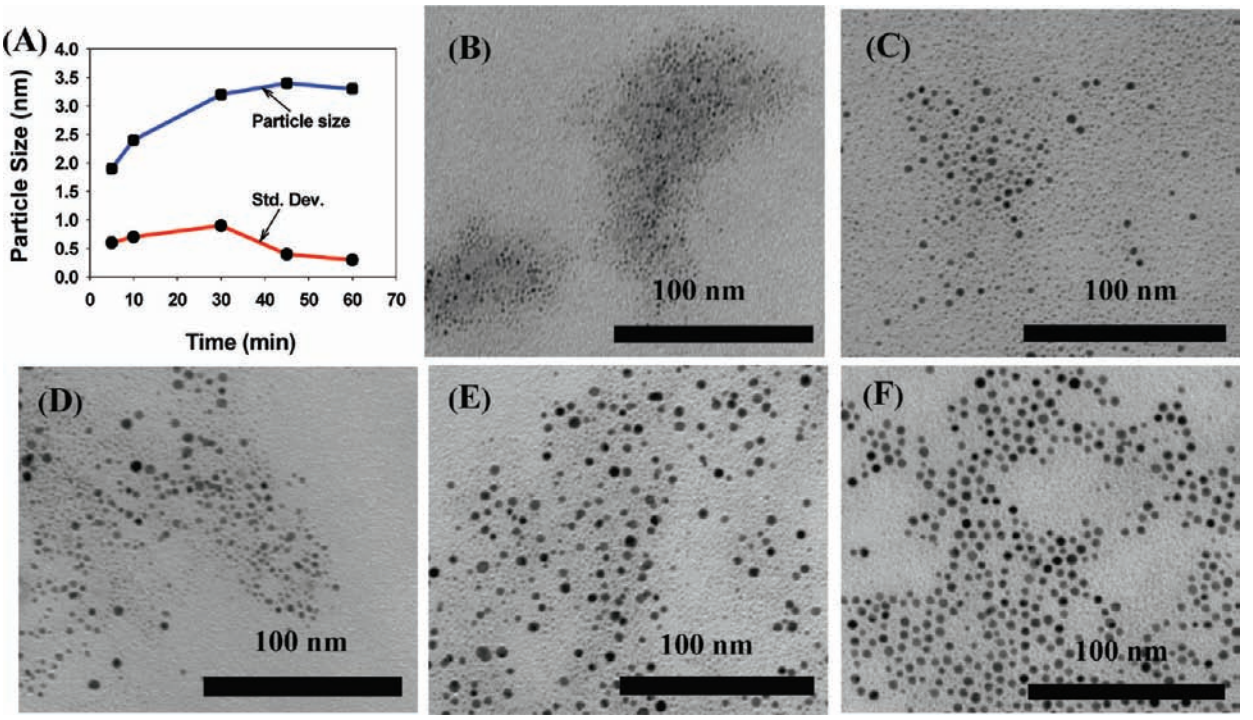

Figure 3. (A) Size and size standard deviation of AuNPs based on TEM analysis. TEM images of particles at time points during synthesis of (B) 2, (C) 5, (D) 10, (E) 30, and (F) 45 min after adding 9-BBN.

three-dimensional (3-D) structure, and as a result information about the variation of height may be lost, leading to shorter observed interparticle distances compared to the true distances and the predicted values.[73]

The reduction and AuNP formation process based on 9-BBN is slow, as observed by the time-dependent UV−vis absorption spectroscopy analysis (Figure 1). We took advantage of the slow nature of this process to use time-dependent TEM analysis to correlate the size and the size dispersion of the AuNPS with the LSPR behavior. Figure 3A shows the trends in the particle size and the size dispersion over the course of the reduction as observed by TEM analysis. Table 1 presents a summary of data from time-dependent UV−vis spectroscopy and TEM analyses. During the course of the reduction process, we observed an initial red shift of the LSPR λ_{max} from 513 nm at 10 min after addition of 9-BBN to 529 nm at 30 min, see Figure 1. In addition to spectroscopic analysis, the size of the AuNPs was analyzed by TEM during this time period (Figure 3). During the initial stage of the reduction, the particles had a large size dispersion of 32%. At 10 min, the average size was 1.9 ± 0.6 nm. Over time, the polydispersity decreased slightly to 28% at 30 min, and the particles had grown to an average size of 3.2 ± 0.9. The increase in the size of the particles correlates with the red shift of the LSPR λ_{max}. At 35 min, we observed a decrease in the LSPR peak amplitude, although the λ_{max} position was unchanged. After this, the average particle size did not change very much, but the size dispersion decreased significantly. For example, after 45 min of the reaction, the particles were only slightly larger than they had been at 30 min with an average size of 3.4 ± 0.4 nm, but the size dispersion had decreased significantly from 28 to 12%. Afterward, continuous blue shifting of the LSPR peak λ_{max} was observed. Finally, at the end of the reduction (65 min), the LSPR peak position was stable at 520 nm, and the average size of the particles was 3.3 ± 0.3 nm, which means at this end point of the formation process, the particles were mostly monodisperse (9% size dispersion).

Table 1. Comparison of UV−Vis Absorption Maxima and Size of AuNPs at Different Time Intervals after Addition of 9-BBN[a]

time (min)	λ_{max} (nm)	particle size (nm)[b,c]	% relative size dispersion
2	featureless	–	–
5	~500	1.9 (0.6)	32
10	513	2.4 (0.7)	29
30	529	3.2 (0.9)	28
45	523	3.4 (0.4)	12
65	520	3.3 (0.3)	9

[a] In each case, 200 particles were counted to determine the size and the size dispersion. [b] The AuNPs were less than 1.0 nm, and we were unable to determine the size due to the very low contrast in the TEM image. [c] The number in parentheses indicates the standard deviation. In the synthesis, 0.05 mmol of Et_3PAuCl and 0.5 mmol of ODT were used.

The changes in the spectral position of the LSPR peak position during the formation of the nanoparticles could be explained based on the AuNP size, the size dispersity, and the growth process as observed in the UV−vis spectroscopy and the TEM analyses. During the initial 30 min, red shifting of the LSPR peak is related to an increase in nanoparticle size from 1.9 to 3.2 nm. One surprising observation was the LSPR λ_{max} blue shift that followed. Typically a blue shift would be associated with either the dissociation of larger nanoparticles to form smaller ones or the changes in the crystallinity of the nanoparticles.[64] However, in this case TEM analysis showed that the average particle size increased from 3.2 to 3.3 nm during this stage. As mentioned above, during the initial 30 min of the AuNP formation process,

Scheme 2. Proposed Stages of AuNP Formation

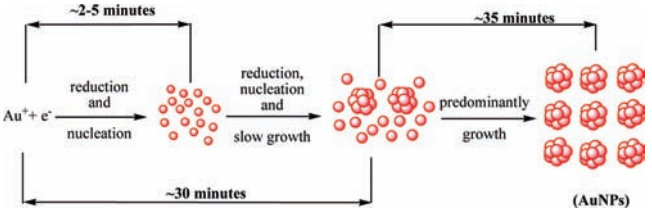

the nanoparticles were quite polydisperse (32% relative size dispersion), and at the end of the synthesis the dispersity decreased to 9%. The observed LSPR λ_{max} blue shifting during the last ~30 min of the AuNP formation process could be due to a decrease of polydispersity from ~28 to ~9%. During this time period, the average size of the nanoparticles was nearly constant at ~3.3 nm, and no changes in the position of the LSPR peak would be expected. However, a narrowing of the LSPR peak as a result of reduced dispersity may lead to an apparent shift due to a change in peak shape. However, we also do not observe significant narrowing of the LSPR peak width. Interestingly Polte et al.[69] reported a LSPR peak blue shift from 540 to 523 nm over the course of gold nanoparticle formation. Scattering studies showed a simultaneous decrease in the total number of particles during the initial stages of the reduction. Then, during later stages of particle growth, the blue-shifting of the LSPR peak continued, even when the particle size increased and the particle density leveled off. There was no experimental evidence of the origin of the blue-shifting of the LSPR peak. In general, particle growth should lead to a red shift of the LSPR peak. In both of these cases, the blue shift may be due to changes in the nanoparticle crystal structure and the surface ligands. Although HRTEM analysis presented later in this article indicates that the particles are single crystalline throughout the reduction process, more systematic and detailed studies of the changes in crystalline structure would need to be done to completely understand this contribution to the LSPR properties. These studies are in progress.

Even without a full understanding of the LSPR behavior, the trends in the nanoparticle size and the size dispersion may be used to characterize the general stages of the gold nanoparticle formation process. By combining the time-dependent spectroscopic and microscopic analyses of the AuNPs, we can begin to elucidate the stages of the AuNP formation process as well as the influence of different reaction parameters on the size and the size dispersion of the AuNPs. The important roles of reduction, nucleation, and growth processes in the formation of metal nanoparticles are well-established.[74] Scheme 2 summarizes the proposed stages of the AuNP formation process based on the time-dependent LSPR data and the TEM analysis. We can distinguish three different stages which take place during the synthesis of the AuNPs using 9-BBN as a reducing agent: (i) a reduction and nucleation step, followed by (ii) simultaneous reduction, nucleation, and slow growth processes, and (iii) a final stage which is predominantly growth of the nanoparticles. At the beginning of the reaction, just after addition of 9-BBN, very small nanosized particles (nuclei) are generated and are the largest population in the TEM image in Figure 3B. Over time, the nuclei grow larger in size via homogeneous nucleation along with formation of more nuclei. The mixture of small particles (nuclei) and larger particles in the TEM images in Figure 3C and D provides evidence for the beginning of a simultaneous nucleation/growth stage which begins 5−10 min after addition of 9-BBN. At that point, the parallel nucleation and growth processes continue until 30 min after 9-BBN addition, as observed in the TEM analysis (see Figure 3E). This is shown by the mixture of ultrasmall nanoparticles along with a population of larger particles of fairly uniform size in the TEM images in Figure 3D and E during the early time periods (10−30 min) of the formation process. The mixture of sizes also is represented by the high standard deviations in particle size observed for those time periods in Table 1. The presence of ultrasmall particles (<1.0 nm) during the first 30 min of the formation process indicates that there must be a constant supply of such particles which serve as nuclei and implies an active nucleation process during that time period. The formation of the larger AuNPs observed in the TEM images for each time point would be possible only if the small size particles experienced a simultaneous growth process that was due to molecular addition, rather than particle aggregation. Further evidence for this growth mechanism is shown by experiments described later in this article. During the 20-min time period of simultaneous growth and nucleation, the rate of nucleation was faster compared to the particle growth rate. This is shown by the larger population of small-sized nanoparticles (nuclei) in the TEM images of the product from this time period. The presence of the large number of nuclei also leads to an increase in the number of larger nanoparticles in solution leading to the rapid increase in LSPR λ_{max} amplitude as observed in the UV−vis spectra (Figure 1). The large size dispersion during the initial particle formation also indicates that the initial stage is governed by rapid nucleation, which typically produces more polydisperse nanoparticles.[69] Over time the concentration of larger particles in the solution decreased as observed by the decrease in the LSPR peak amplitude, while the average particle size increased. This indicates that the growth process played a greater role at later stages, as would be expected, reducing the particle size dispersity. Particle growth plays an important role as the reduction process using 9-BBN proceeds more slowly than the traditional sodium citrate or borohydride methods. As a result, the nuclei which are formed in the initial stage of the reduction process undergo a slower growth step. The final stage of the reduction process was dominated by nanoparticle growth shown by the generation of nearly monodisperse particles. The TEM analysis (Figure 3C and D) supports the observed LSPR behavior where the concentration of ultrasmall particles is much higher than the larger particles observed at each time point. At 30 min after addition of 9-BBN, the nucleation process was complete, and after that nanoparticle formation was dominated by growth, which produced the monodisperse AuNPs. Our observations correlate with those presented by Peng et al. which also showed that during the nanoparticle growth process, small size clusters grow faster than the larger ones, narrowing down the size distribution over the time course of nanoparticle formation.[75] More detailed discussions of the nanoparticle growth process are in the following section.

In order to determine the nature of the growth process, we analyzed the samples at various stages during the reduction reaction using HRTEM. Figure 4 shows the HRTEM images of AuNPs produced by 9-BBN reduction at different stages of particle formation. The nanoparticles appear to be predominantly single crystalline (~99%) in structure at various stages of the reduction process (see Supporting Information Figures 2−7 for additional HRTEM images). The crystallinity of the

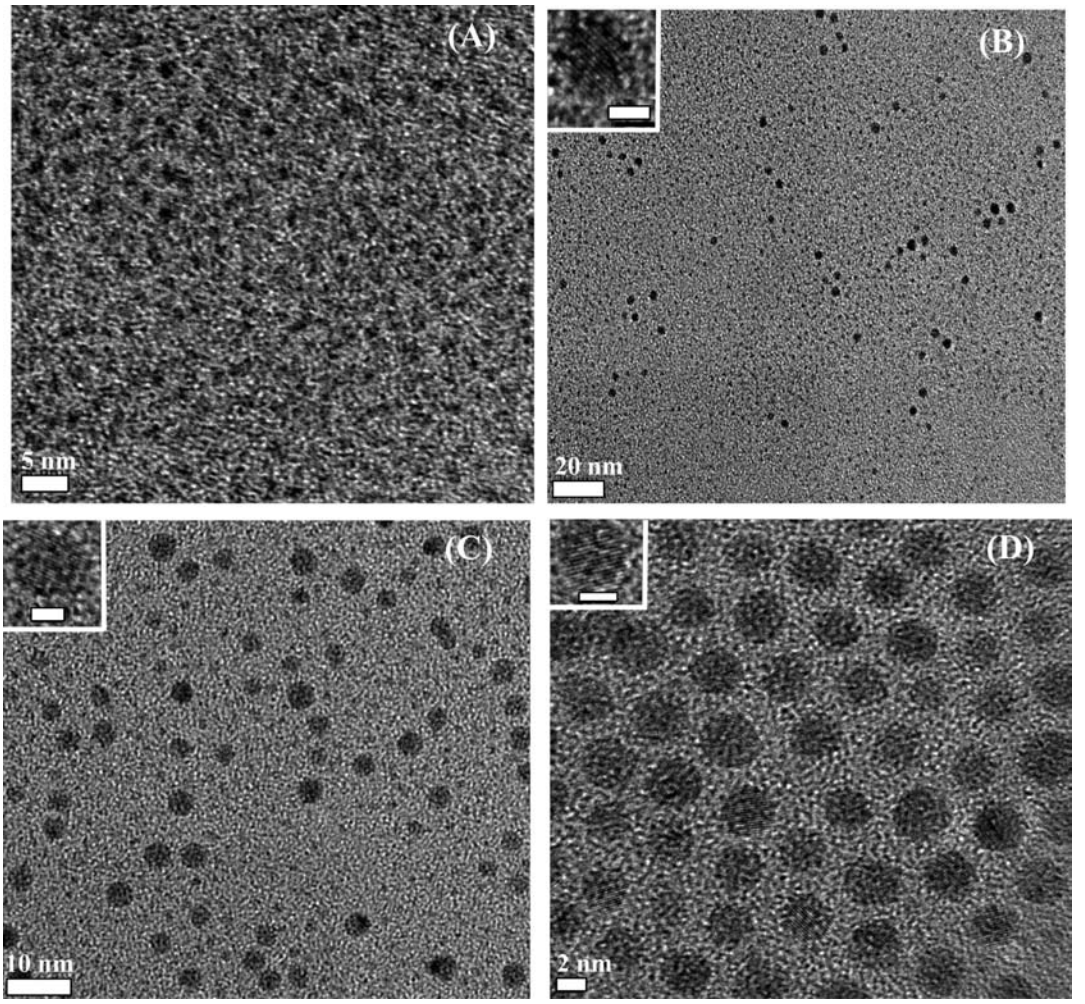

Figure 4. HRTEM images of particles at time points during synthesis of: (A) 2, (B) 5, (C) 30, and (D) 65 min after adding 9-BBN. Insert in B−D shows single nanoparticle image with a scale bar of 2 nm. The images clearly show single crystalline lattice planes.

nanoparticles suggests that the growth of the particles follows a classical diffusion controlled Ostwald-ripening mechanism.[76] In a recent report by Buhro and co-workers, two different growth mechanisms for formation of thiol-protected AuNPs were described: (i) aggregative and (ii) Ostwald ripening.[77] An aggregative growth mechanism produces primarily polycrystalline AuNPs. On the other hand, single crystalline AuNPs are expected if the growth process follows an Ostwald-ripening mechanism, which appears to be the case for the 9-BBN-based AuNP synthesis according to the HRTEM analysis.

The important role of diffusion-limited growth in the synthesis of monodisperse nanoparticles with less than 10% size dispersion is well established.[75] During a diffusion-limited growth process, molecular addition is facilitated where active nuclei adsorb on the surfaces of larger particles. This growth mechanism generally occurs for chemical reactions where the supply of growth species is slow. In addition, the supply of capping ligand also is essential. The surface-bound capping ligands form a diffusion barrier, which hinders adsorption and further growth of the nanoclusters. In this present investigation, the AuNPs grew from very polydisperse (32%) particles with an average size of 1.9 ± 0.6 nm to monodisperse (9%) particles with an average size of 3.3 ± 0.3 nm. The UV−vis spectroscopy analysis showed initial red shifts followed by blue shifts of the LSPR λ_{max} of the AuNPs. The red shifts are due to the increase of particle size from 1.9 to 3.2. In the remaining 30 min of the reduction process, a very small particle size increase (∼0.1 nm) was observed, but the dispersity decreased much more significantly from 28 to 9% with a final AuNP size of 3.3 nm. Alivisatos and co-workers observed a similar change in size dispersion, from highly polydisperse to nearly monodisperse particles, over the time course of PtNP formation using in situ HRTEM analysis.[65] Their results indicated that at the beginning of the reduction process a large number of nanocrystals were formed which undergo parallel nucleation and growth processes. The size distribution of particles was large at the beginning, followed by a bimodal distribution during the nucleation/growth stage. At the end of the formation process, the size distribution was narrow, and monodisperse nanoparticles were observed. These observations may be explained by a classical diffusion-controlled growth mechanism, and this is discussed more below. As discussed above, the observations made for the gold nanoparticle formation process based on 9-BBN as a reducing agent are similar to their findings.

Effects of Stabilizing Agent Concentration. We investigated the influence of the concentration of the stabilizing agent (ODT) on the reaction rate and the size of the AuNPs. In these studies,

we varied the Au(I) to thiol mole ratio by changing the amount of ODT while keeping the reaction temperature and amounts of Et_3PAuCl and 9-BBN constant. We observed that when lower amounts of thiol were used, the AuNPs formed faster compared to when higher amounts of thiols were included in the reaction mixture. For example, in the presence of 0.12 mmol of ODT, the reaction took 30 min to reach a stable absorption maximum (LSPR λ_{max} peak amplitude), and the time to reach completion increased to 165 min when 2.50 mmol of ODT was used for nanoparticle synthesis, see Table 2. The final size of the AuNPs produced depends on the amount of ODT used. We observed that larger AuNPs were formed when higher amounts of ODT were used, and smaller AuNPs were produced in the presence of lower amounts of ODT, which is shown by the TEM images in Figure 5A and D and the data in Table 2. In the case of $NaBH_4$-based two-phase syntheses, literature reports have indicated that the amount of stabilizing agent, in most cases thiol ligands present in the reaction mixture, significantly influences the size of the synthesized AuNPs.[53] In related work, Murray and co-workers have reported that different sizes of AuNPs stabilized by hexanethiolate ligands also can be synthesized by changing the Au(III)-to-thiol mole ratios.[78] In their reports, 2.2, 2.0, and 1.6 nm AuNPs were synthesized at room temperature when the corresponding gold-to-ligand mole ratios were 1:1, 1:2, and 1:3, respectively.[78] However, we observed the opposite behavior as 2.6, 3.3, 3.8, and 4.3 nm AuNPs were formed when Au(I)-to-thiol mole ratios were 1:2.4, 1:5, 1:20, and 1:50, respectively. The influence of amount of ODT on the particle size is due to complex formation with 9-BBN which reduces the amount of hydride available to participate in the reduction process, leading to the production of smaller nanoparticles in the presence of larger amounts of ODT. This is discussed in more detail later in this article.

Table 2. Comparison of Reaction Time, LSPR λ_{max}, and Size of Gold Nanoparticles Synthesized Using Different Amounts of ODT[a]

[ODT] (mmol)	time for stable λ_{max} (min)	λ_{max} (nm)	particle size (nm)[b]
0.12	30	516	2.6 (0.5)
0.25	45	518	3.3 (0.4)
0.50	65	520	3.3 (0.3)
1.00	90	520	3.8 (0.7)
2.50	165	526	4.3 (0.9)

[a] In each case, at least 200 particles were counted to determine the size and the size dispersion. The syntheses were carried out using 0.017 g (0.05 mmol) of Et_3PAuCl, 0.2 mL of 0.5 M 9-BBN in THF, and catalytic amount 0.005 mL (0.01 mmol) of TOA. [b] The number in parentheses indicates the standard deviation. The syntheses of AuNPs in the presence of various amounts of thiols were carried out at room temperature.

Interestingly, we have observed that the LSPR properties of the synthesized AuNPs also were influenced by the amount of ODT present in the reaction mixture. Previously Whetten and co-workers reported that the optical absorption properties[9] of thiol protected gold clusters are highly sensitive to the size of the metallic core of the cluster assembly. Also, as the size of the AuNPs increases, the LSPR λ_{max} is expected to shift to longer wavelengths. We investigated the LSPR properties of the AuNPs synthesized using 9-BBN in the presence of various amounts of ODT. The observed LSPR properties of the particles showed a dependence on the amount of ODT. Table 2 presents a summary

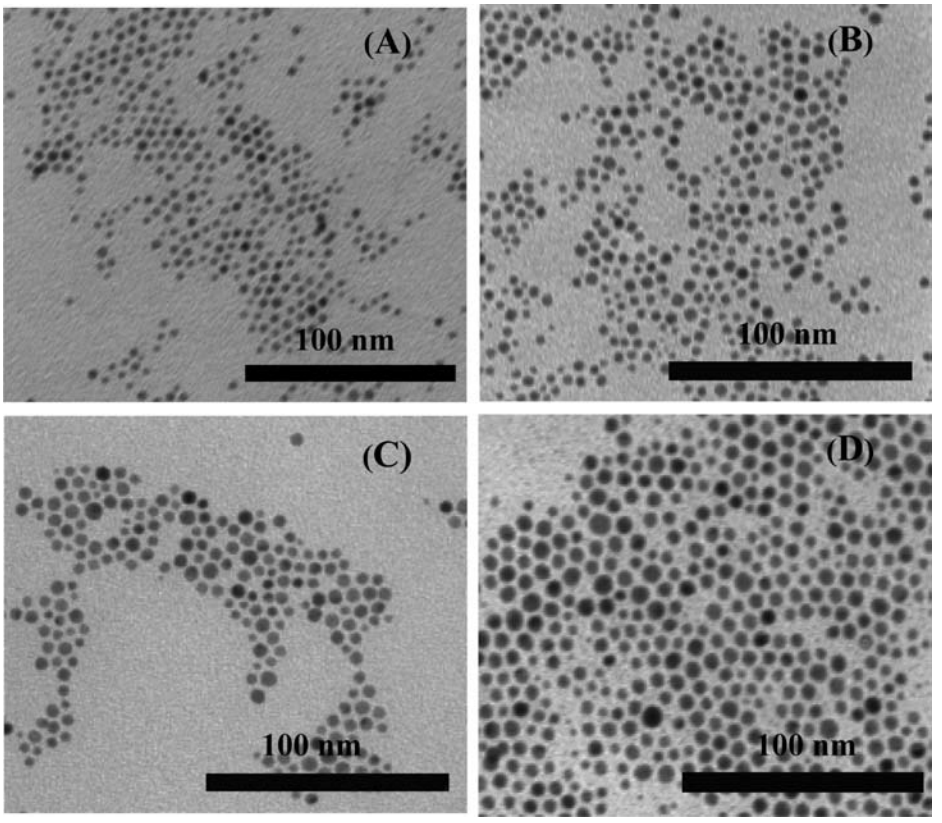

Figure 5. TEM images of AuNPs synthesized in the presence of different amounts of ODT: (A) 0.12, (B) 0.25, (c) 1.00 and (D) 2.50 mmol.

Scheme 3. Reaction Pathway between Alkylthiols and 9-BBN

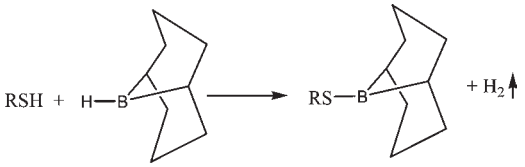

of the spectroscopic and the microscopic characterization including the time it took for the LSPR peak to reach a stable amplitude, the corresponding λ_{max} (wavelength) values, and the size of the AuNPs synthesized using different amounts of ODT. Representative TEM images of AuNPs synthesized in the presence of different amounts of ODT are shown in Figure 5. Depending on the amount of thiol present in the solution, the λ_{max} varied from 516 to 526 nm when all other reaction conditions were the same. The amplitude of the LSPR peak was lowest in the case of lower amounts (0.12 mmol) of ODT, where the observed LSPR λ_{max} was 516 nm. The LSPR peak red shifted to 526 nm when 2.25 mmol of ODT was used for nanoparticle synthesis. The corresponding TEM analysis showed much smaller (diameter of 2.6 nm, Figure 5A) AuNPs were produced in the presence of a lower amount (0.12 mmol) of ODT compared to the larger (4.3 nm, Figure 5D) AuNPs formed when 2.50 mmol of ODT was used. The TEM analysis correlates with the UV−vis analysis, where 2.6 and 4.3 nm AuNPs displayed LSPR absorption peaks at 516 and 526 nm, respectively. As expected, the LSPR peak red shifted as the size of the AuNPs increased. In addition, with an increase in Au(I)-to-thiol ratio, the particles are more polydisperse in nature, and this is discussed below.

We have shown that, for a given molar amount of metal salt and reducing agent, the time to reach a stable absorption maximum in the LSPR peak was dependent on the amount of capping ligand, ODT, present in the reaction mixture. The slow formation of AuNPs in the presence of higher concentrations of ODT has provided us the opportunity to investigate the reducing character of 9-BBN, including the role of complex formation with alkylthiolates and the potential impact on hydride formation. Previously, Brown and co-workers have shown that thiol-terminated primary or secondary alkyl hydrocarbons form complexes with hydroborating agents and rapidly liberate hydrogen gas.[79,80] In the case of 9-BBN, the reaction is shown in Scheme 3.

Due to this complex formation, the reaction mixture eventually will lack hydrides which reduce metal ions to atoms in the AuNP synthesis. In our system, we have observed that in the presence of a lower amount (0.12−0.5 mmol) of ODT, the particle formation is faster and completed within 30−65 min after addition of 9-BBN. With an increase in the molar amount of thiol in the reaction mixture, the rate of AuNPs was observed to be slower. For example, in the presence of 2.5 mmol of 9-BBN, the reduction took ∼165 min to reach a stable λ_{max}. The high ODT concentration is expected to reduce the hydride concentration in the solution and liberate hydrogen gas. Nanoparticle formation rate will be reduced due to the lack of hydride. The experimental evidence from UV−vis spectroscopy analysis suggests that the complex formation between 9-BBN and excess thiols significantly influences steps (i) and (ii) in Scheme 2.

Temperature Effects on Reaction Rate and Particle Size. We investigated the effect of temperature on the size, size dispersity, and LSPR properties of the AuNPs. The AuNPs were

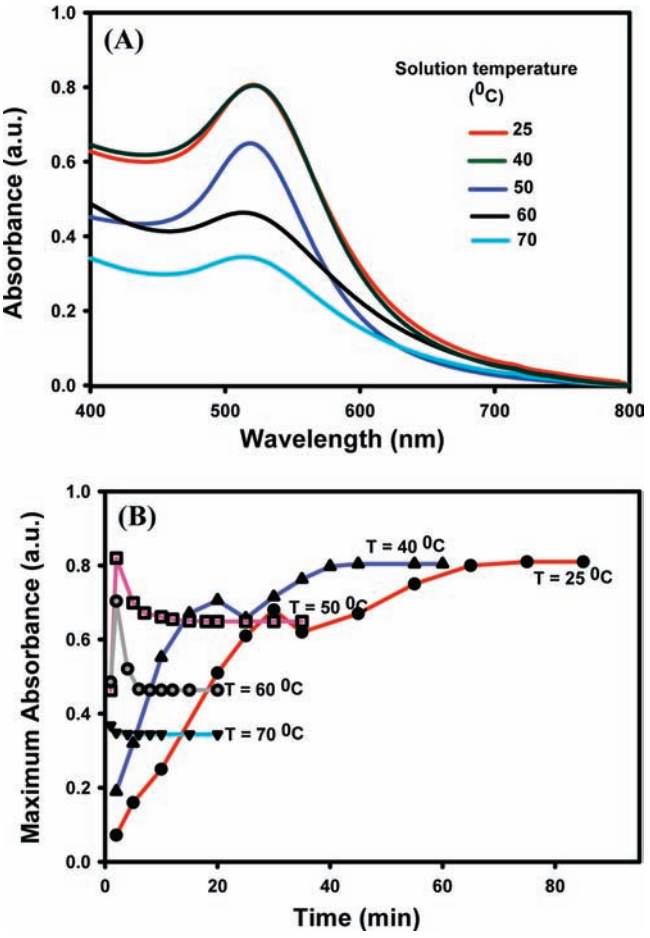

Figure 6. (A) UV−vis absorption spectra of AuNPs synthesized at different reaction temperatures and (B) the rates of nanoparticle formation from spectroscopy analysis at different time intervals at various solution temperatures.

synthesized at solution temperatures ranging from 25 to 70 °C according to the synthetic procedure described in the Experimental Section. The reaction progress was monitored by UV−vis spectroscopy, and as soon as the reaction mixture displayed a stable LSPR λ_{max}, the solution was removed from heat and allowed to cool to room temperature. We observed that the formation of AuNPs using 9-BBN is strongly temperature dependent. As the solution temperature increased, the generation of AuNPs was faster, as observed by the λ_{max} reaching a stable value more rapidly, with the particle formation time decreasing from 65 min at 25 °C to 5 min at 70 °C. Figure 6A presents the UV−vis absorption spectra of AuNPs synthesized at different reaction temperatures. As we see from the spectra, the LSPR λ_{max} blue shifted as the reaction temperature increased. Based on this blue shift, we would expect the average particle size at higher temperature to be smaller. In order to compare the LSPR properties of the AuNPs with particle size, we performed TEM analysis. Figure 7 presents representative TEM images of nanoparticles synthesized at different temperatures. The TEM analysis shows nanoparticles are almost monodisperse with average diameters of 3.3−1.5 nm for the temperatures used. The sizes at 25 and 40 °C are in the range of 3 nm and decrease to 2 nm when the reduction took place at 50 or 60 °C. On the other hand, when the reduction was performed at 70 °C, the particles

dx.doi.org/10.1021/ja107934h |J. Am. Chem. Soc. 2011, 133, 8179–8190

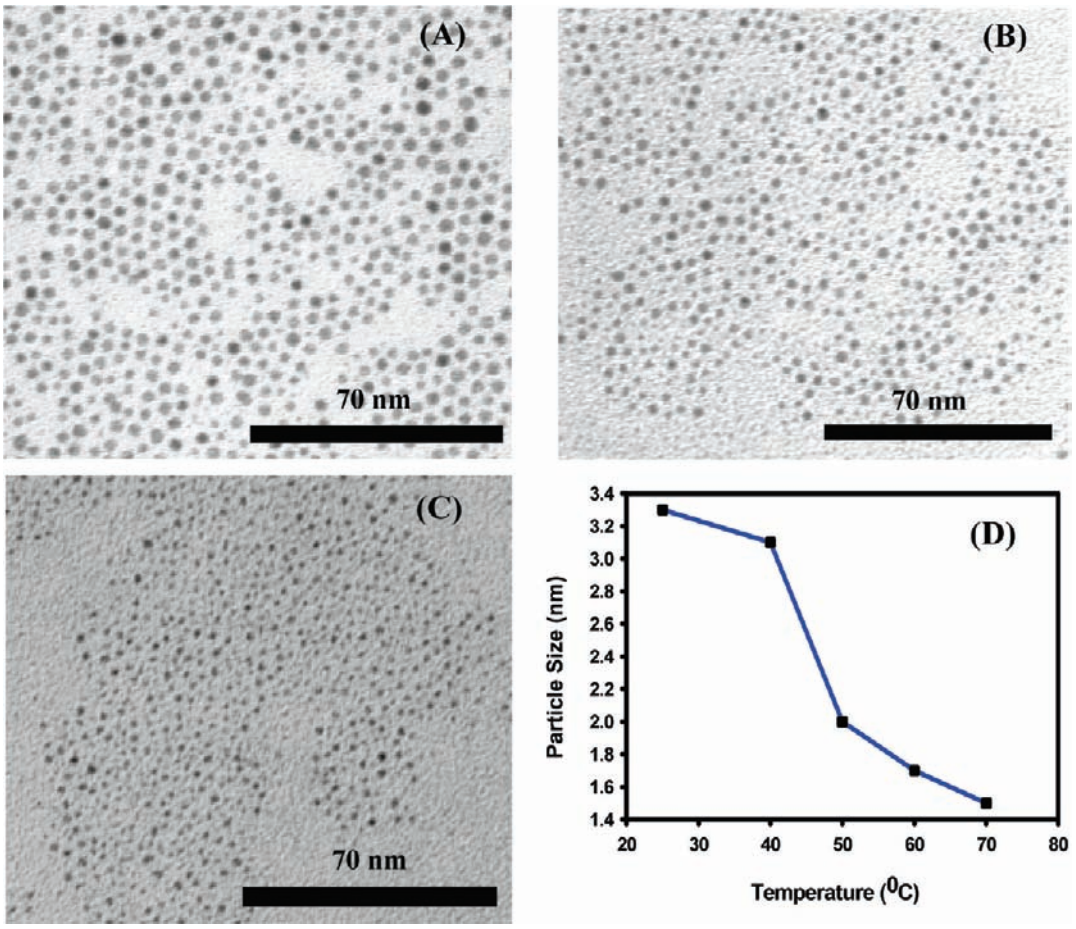

Figure 7. TEM images of AuNPs synthesized at solution temperatures of (A) 50, (B) 60, and (C) 70 °C. (D) Particle size dependence on solution temperature.

are nearly monodisperse in nature (<10% dispersity) with average diameter of 1.5 nm. The decrease in the average size of particles prepared at higher temperature correlates with the observed shifting of the LSPR λ_{max} to shorter wavelengths.[9] Analysis shows batches of particles with average sizes of 3.2 and 1.5 nm displayed LSPR λ_{max} values of 520 and 512 nm, respectively (see Table 1). In addition to the blue shifts of the LSPR peak position, we also observed a decrease in LSPR peak amplitude as the solution temperature increased. The 1.5 and 3.2 nm ODT protected nanoparticles show the lowest and highest values of peak amplitude, respectively. This observation is in agreement with Whetten and co-workers[9] and Hussain et al.[81] who also have reported that when AuNPs were coated with thiolate ligands, the amplitude of the absorption maxima decreased as the nanoparticle size decreased. This is due to the ligand influence on the electronic properties of the particles in addition to the size dependence of the scattering and absorption cross sections for the particles. In this present investigation, we believe this could be the reason for the decrease of the LSPR peak amplitude where the nanoparticle size decreased from 3.2 to 1.5 nm as the solution temperature increased from 25° to 70 °C.

As we discussed above, the solution temperature substantially influenced the generation of AuNPs. The formation of the nanoparticles was faster as observed by the λ_{max} reaching a stable value more quickly as we increased the reaction temperature. We used UV−vis absorption spectroscopy to investigate the kinetics of nanoparticle formation at different time intervals, as shown by the spectra in Figure 6B. Based on the UV−vis spectroscopy analysis, we found that both the nucleation and the growth processes are significantly influenced by the reduction of temperature, and three different trends in the kinetic behavior related to particle formation are observed: (i) When the reactions were performed at 25° and 40 °C, the trends of the absorption spectra related to the AuNPs produced are comparable, where a steady increase in the LSPR peak amplitude was observed until the 30- and 20-minute time points, respectively. In both cases, the amplitude of LSPR peak then decreased for ∼5 min and again slowly increased until reaching stable maxima after 65 and 60 min for the 25 and 40 °C reactions, respectively. The evaluation of LSPR λ_{max} peak wavelength shifts for synthesis at 25 °C was described earlier in the article. We also observed similar trends in the LSPR peak position when the synthesis was performed at 40 °C. At this temperature, the LSPR λ_{max} peaks red shifted until ∼20 min after addition of 9-BBN and then blue shifted until the LSPR peak stabilized. More detailed high-resolution structural analysis of the AuNPs is underway to identify the origin of the blue shifting the LSPR peak. (ii) For syntheses carried out at 50 and 60 °C, the amplitude of the LSPR peak increased more quickly and reached the maximum value within 2 min. The amplitudes of the LSPR λ_{max} peaks then decreased for another ∼10 min until stable absorption maxima were observed after approximately 15 and 8 min, respectively, after addition of

Table 3. Summary of UV−Vis Spectroscopy and TEM Characterization of AuNPs Synthesized at Different Solution Temperatures[a,b]

temp (°C)	time for stable λ_{max} (min)	λ_{max} (nm)	particle size (nm)[c]
25	65	520	3.3 (0.3)
40	45	520	3.1 (0.3)
50	15	518	2.0 (0.3)
60	8	512	1.7 (0.2)
70	5	512	1.5 (0.2)

[a] In each case, at least 200 particles were analyzed to determine the size and the size dispersion. [b] The syntheses were carried out using 0.017 g (0.05 mmol) of Et_3PAuCl, 0.17 mL (0.5 mmol) of ODT, 0.2 mL of 0.5 M 9-BBN in THF, and a catalytic amount of 0.005 mL (0.01 mmol) of TOA. [c] The number in parentheses indicates the standard deviation.

9-BBN. In those cases, only LSPR λ_{max} blue shifts were observed. (iii) When the reduction was performed at 70 °C, the formation of nanoparticles was very fast, and in this case, one minute after addition of 9-BBN addition, the LSPR λ_{max} peak amplitude decreased by 0.02 au and then stabilized within 5 min after addition of reducing agent.

The time-dependent kinetics data (Figure 6B) and TEM results (Figures 4 and 7) clearly suggest that the nucleation and the growth processes contribute differently to the AuNP formation process as the reaction temperature is varied: (i) When the reduction was performed at 25 and 40 °C, the formation of AuNPs followed the process discussed in more detail above and illustrated by Scheme 2. In this case, the particle formation process consists of a reduction-nucleation stage, a simultaneous reduction, nucleation, and growth stage, and a final growth stage. (ii) More rapid nucleation plays an important role when the reduction reactions were performed at either 50 or 60 °C. Figure 6B suggests that after addition of 9-BBN to the reaction mixture, an immediate reduction of Au(I) ions took place, and the solution contained a high concentration of active nuclei. Due to presence of a large number of active nuclei, one would expect a short nucleation time period, and we assume in this case that this step was completed within 5 min after addition of reducing agent, and then the system went through a complete growth process for another 5−10 min. During the growth, dissolution of smaller particles and addition of the material on the surface of larger nanoparticles likely take place. In this period, consequently the numbers (concentration) of nanoparticles in the solution decreased, which affected the optical behavior of the particles and led to a decrease in the LSPR peak amplitude. (iii) At the higher temperature, 70 °C, the reduction, nucleation, and growth processes occurred simultaneously and very quickly as observed by the LSPR peak amplitude reaching a stable maximum value at ∼6 min after addition of 9-BBN. The formation of AuNPs at 70 °C using 9-BBN is more similar to the Brust two-phase synthetic approach where reduction, nucleation, and growth processes take place within milliseconds to a few seconds time frame after the addition of a reducing agent (i.e., $NaBH_4$ in the case of the Brust method).[68,69] Real-time monitoring of nanoparticles formation process via light scattering techniques would provide better information regarding the differences in growth mechanisms at different reduction temperatures.

In addition to differences in the size and the size dispersion of AuNPs produced at different temperatures, we observed that the ordered assembly of the particles on the TEM grid is strongly reaction temperature dependent. The AuNPs synthesized at 25 and 40 °C displayed a close-packed 2-D assembly with regular interparticle spacing of ∼2.2 nm, and the detailed observations are explained earlier in this article. On the other hand, with an increase of the solution temperature to 50 °C, the 2-D assembly was less ordered as shown in the TEM image in Figure 7. At higher temperatures, i.e., 60 or 70 °C, the particles were randomly dispersed on the TEM grid, and no short-range order was observed, see Figure 7B and C. The dependence of the ordered assembly on reaction temperature may be linked to the packing of the alkylthiolates on the AuNPs. When the nanoparticles were synthesized at 60 or 70 °C, the alkyl chains may have been more disordered due to the higher temperature favoring less-organized packing compared to more-ordered packing when the particles form over a longer time period at lower temperatures. Also at higher temperatures, place exchange could take place between the surface-bound thiolated ligands and the free thiols present in the solution.[28−30,53] This process could also disturb the ligand packing on the surface of the particle. Overall, a more disordered ligand arrangement on the surfaces of the AuNPs could significantly influence the packing and short-range order of the nanoparticles. Lennox and co-workers have extensively studied the nature of alkyl chains of C_{18}−SH thiols packing when the molecules are bound to the gold nanoparticle surface.[68,69] They observed that at temperatures of 25 °C or higher, the thiolated alkyl chains mostly exist in an extended all-trans ordered conformation.[82] The spectroscopic characterization shows that with an increase of temperature, the highly ordered alkyl chains became more disordered in nature. In addition, there were significant numbers of mobile ligands present at higher temperature.[83,84] In the case of 9-BBN induced AuNPs synthesis at elevated temperature, e.g. 60 or 70 °C, the contribution of disordered alkyl chains, continuous place exchange reactions, and migration of thiolated ligands would lead to less particle organization.

Correlation of Particle Size and Size Dispersion with Rate of Nucleation and Growth Time. We have discussed the nanoparticle formation process dependence on concentration of stabilizing ligand (ODT) present and solution temperature. In this section, we discuss the correlation of these reaction parameters with the size and the size dispersion of the AuNPs. We relate the particle size with the stages of the nanoparticle growth including the rate of nucleation and the growth time, which may be correlated with the nanoparticle size and size dispersion. In the case of 9-BBN induced synthesis of AuNPs at room temperature in the presence of different amounts of ODT, the reduction takes longer in the presence of higher amount of thiols and vice versa. This was observed by the differences in reaction time required to reach a stable LSPR absorption maximum. A shorter time was observed for a lower amount of ODT, and it took a longer time when a greater amount of ODT was used. The higher amount of thiols reduced the rate of active nuclei. This is likely caused by a reduction in the hydride present in the reaction mixture as explained above. As a result both the nucleation and the growth processes also were slower. As expected, the slow nucleation process leads to generation of more polydisperse particles, which is what we observed for AuNPs formed in the presence of 2.5 mmol of ODT. Moreover, the larger average size of the nanoparticles prepared in the presence of a higher amount of ODT could be due to a slower particle growth process, which correlates with the observation that the size of the AuNPs is proportional to the growth time. The sizes of the nanoparticles

were 2.6 ± 0.5 and 4.3 ± 0.9 nm for 0.12 and 2.5 mmol of ODT, respectively, see Table 2. Previously, it also was reported that for homogeneous nucleation the size dispersity of nanoparticles depends on the nucleation rate.[75] In the case of fast nucleation, the system generates monodisperse particles. In addition, based on a classical diffusion-controlled Ostwald-ripening growth mechanism, the size of the nanoparticles is expected to be proportional to the growth time.[65,76] However, in the presence of high concentrations of ODT (2.5 mmol), the AuNP formation was slower (165 min) and resulted in polydisperse AuNPs due to the slow nucleation and growth processes.

The temperature effects on particle size and size dispersion also can be interpreted based on the rate of nucleation and growth processes. At lower temperatures of 25 and 40 °C, the times for the formation of stable absorption maxima were 65 and 45 min, respectively. These lower temperatures and longer reaction times produced nanoparticles with an average size of ~3 nm. However, the size of the nanoparticles was reduced to 2.0 and 1.7 nm when the reduction reactions were performed at 50 and 60 °C, respectively. At these higher temperatures, the reaction proceeded more quickly with stable absorption maxima observed 8 to 15 min after addition of 9-BBN, depending on the temperature used. The kinetic data correlate with the final size of the AuNPs. The rapid formation of active nuclei at higher temperature (50 and 60 °C) substantially promotes the nucleation and the growth steps resulting in formation of smaller, nearly monodisperse AuNPs. The very fast nucleation and growth processes lead to the very small 1.5 nm AuNPs at 70 °C where a stable absorption maximum was observed ~5 min after addition of 9-BBN. The experimental results from both UV−vis absorption and TEM analysis show the correlation between the size and the size dispersion of AuNPs and the stabilizing agent concentration as well as the solution temperature.

CONCLUSION

The slow AuNP formation based on using 9-BBN as a reducing agent enabled investigations of the relationship between reaction parameters and the size and size dispersion of AuNPs based on simple UV−vis spectroscopy and TEM analyses. We demonstrated synthesis of nearly monodisperse AuNPs in organic solvents. The HRTEM analysis showed the nanoparticles are mostly single crystalline in nature, which is likely due to a dominant diffusion-controlled Ostwald-ripening growth mechanism. The amounts of capping ligand and the reduction temperature have an important impact on nucleation and growth processes which directly influence the final sizes of the nanoparticles. By identifying different stages of AuNP formation, we can begin to try to control the formation process by manipulating conditions to favor specific stages of reduction, nucleation, and growth over the time course of the AuNP formation. This investigation demonstrates the use of simple approaches to gain a more detailed characterization of nanoparticle formation and provides important insight into the stages of the nucleation and growth during the borohydride-based synthesis of thiolate-stabilized AuNPs. More detailed studies, including in situ characterization of AuNP crystallinity, using small-angle X-ray scattering (SAXS) and selected area electron diffraction (SAED), should provide additional information impacting fundamental understanding of nanoparticle formation and are underway. These investigations also should form a good basis for tailoring reaction conditions to tune the particle characteristics, such as size, size dispersion, crystalline structure, and shape.

ASSOCIATED CONTENT

Supporting Information. ^{1}H NMR of purified ODT stabilized AuNPs and additional HRTEM images. This material is available free of charge via the Internet at http://pubs.acs.org.

AUTHOR INFORMATION

Corresponding Author

shumaker-parry@chem.utah.edu

Present Addresses

[†]Department of Chemistry and Chemical Biology, Indiana University−Purdue University Indianapolis, 402 N. Blackford Street, Indianapolis, IN 46202, United States.

ACKNOWLEDGMENT

We would like to thank Dr. Amar Khumbar at UNC-Chapel Hill for assistance with HRTEM analysis.

REFERENCES

(1) Katz, E.; Willner, I. *Angew. Chem., Int. Ed.* **2004**, *43*, 6042–6108.
(2) Taton, T. A.; Mirkin, C. A.; Letsinger, R. L. *Science* **2000**, *289*, 1757–1760.
(3) He, L.; Musick, M. D.; Nicewarner, S. R.; Salinas, F. G.; Benkovic, S. J.; Natan, M. J.; Keating, C. D. *J. Am. Chem. Soc.* **2000**, *122*, 9071–9077.
(4) Maier, S. A.; Kik, P. G.; Atwater, H. A.; Meltzer, S.; Harel, E.; Koel, B. E.; Requicha, A. A. G. *Nat. Mater.* **2003**, *2*, 229–232.
(5) Novak, J. P.; Brousseau, L. C.; Vance, F. W.; Johnson, R. C.; Lemon, B. I.; Hupp, J. T.; Feldheim, D. L. *J. Am. Chem. Soc.* **2000**, *122*, 12029–12030.
(6) Pissuwan, D.; Valenzuela, S. M.; Cortie, M. B. *Trends Biotechnol.* **2006**, *24*, 62–67.
(7) Enache, D. I.; Edwards, J. K.; Landon, P.; Solsona-Espriu, B.; Carley, A. F.; Herzing, A. A.; Watanabe, M.; Kiely, C. J.; Knight, D. W.; Hutchings, G. J. *Science* **2006**, *311*, 362–365.
(8) Tsunoyama, H.; Sakurai, H.; Negishi, Y.; Tsukuda, T. *J. Am. Chem. Soc.* **2005**, *127*, 9374–9375.
(9) Alvarez, M. M.; Khoury, J. T.; Schaaff, T. G.; Shafigullin, M. N.; Vezmar, I.; Whetten, R. L. *J. Phys. Chem. B* **1997**, *101*, 3706–3712.
(10) Bao, Y.; Zhong, C.; Vu, D. M.; Temirov, J. P.; Dyer, R. B.; Martinez, J. S. *J. Phys. Chem. C* **2007**, *111*, 12194–12198.
(11) Lopez-Acevedo, O.; Tsunoyama, H.; Tsukuda, T.; Häkkinen, H.; Aikens, C. M. *J. Am. Chem. Soc.* **2010**, *132*, 8210–8218.
(12) Provorse, M. R.; Aikens, C. M. *J. Am. Chem. Soc.* **2010**, *132*, 1302–1310.
(13) Aikens, C. M. *J. Phys. Chem. C.* **2008**, *112*, 19797–19800.
(14) Bukasov, R.; Shumaker-Parry, J. S. *Nano Lett.* **2007**, *7*, 1113–1118.
(15) Burda, C.; Chen, X.; Narayanan, R.; El-Sayed, M. A. *Chem. Rev.* **2005**, *105*, 1025–1102.
(16) El-Sayed, M. A. *Acc. Chem. Res.* **2001**, *34*, 257–264.
(17) Habas, S. E.; Lee, H.; Radmilovic, V.; Somorjai, G. A.; Yang, P. *Nat. Mater.* **2007**, *6*, 692–697.
(18) Henzie, J.; Shuford, K. L.; Kwak, E. S.; Schatz, G. C.; Odom, T. W. *J. Phys. Chem. B* **2006**, *110*, 14028–14031.
(19) Jana, N. R.; Gearheart, L.; Murphy, C. J. *Langmuir* **2001**, *17*, 6782–6786.
(20) Kim, F.; Song, J. H.; Yang, P. *J. Am. Chem. Soc.* **2002**, *124*, 14316–14317.

(21) Millstone, J. E.; Park, S.; Shuford, K. L.; Qin, L.; Schatz, G. C.; Mirkin, C. A. *J. Am. Chem. Soc.* **2005**, *127*, 5312–5313.
(22) Sau, T. K.; Murphy, C. J. *J. Am. Chem. Soc.* **2004**, *126*, 8648–8649.
(23) Shankar, S. S.; Rai, A.; Ankamwar, B.; Singh, A.; Ahmad, A.; Sastry, M. *Nat. Mater.* **2004**, *3*, 482–488.
(24) Ghosh, S. K.; Kundu, S.; Nath, S.; Pal, T. *Appl. Spectrosc.* **2005**, *59*, 844–847.
(25) Kelly, K. L.; Coronado, E.; Zhao, L. L.; Schatz, G. C. *J. Phys. Chem. B* **2003**, *107*, 668–677.
(26) Lazarides, A. A.; Schatz, G. C. *J. Phys. Chem. B* **2000**, *104*, 460–467.
(27) Miller, M. M.; Lazarides, A. A. *J. Phys. Chem. B* **2005**, *109*, 21556–21565.
(28) Hostetler, M. J.; Zhong, C. J.; Yen, B. K. H.; Anderegg, J.; Gross, S. M.; Evans, N. D.; Porter, M.; Murray, R. W. *J. Am. Chem. Soc.* **1998**, *120*, 9396–9397.
(29) Templeton, A. C.; Wuelfing, W. P.; Murray, R. W. *Acc. Chem. Res.* **2000**, *33*, 27–36.
(30) Wuelfing, W. P.; Gross, S. M.; Miles, D. T.; Murray, R. W. *J. Am. Chem. Soc.* **1998**, *120*, 12696–12697.
(31) Hickman, J. J.; Ofer, D.; Laibinis, P. E.; Whitesides, G. M.; Wrighton, M. S. *Science* **1991**, *252*, 688–691.
(32) Guo, R.; Song, Y.; Wang, G.; Murray, R. W. *J. Am. Chem. Soc.* **2005**, *127*, 2752–2757.
(33) Song, Y.; Murray, R. W. *J. Am. Chem. Soc.* **2002**, *124*, 7096–7102.
(34) Brennan, J. L.; Branham, M. R.; Hicks, J. F.; Osisek, A. J.; Donkers, R. L.; Georganopoulou, D. G.; Murray, R. W. *Anal. Chem.* **2004**, *76*, 5611–5619.
(35) Deng, F.; Yang, Y.; Hwang, S.; Shon, Y,-S.; Chen, S. *Anal. Chem.* **2004**, *76*, 6102–6107.
(36) Yang, Y.; Chen, S. *Nano Lett.* **2003**, *3*, 75–79.
(37) Chaki, N. K.; Singh, P.; Dharmadhikari, C. V.; Vijayamohanan, K. P. *Langmuir* **2004**, *20*, 10208–10217.
(38) Hicks, J. F.; Templeton, A. C.; Chen, S.; Sheran, K. M.; Jasti, R.; Murray, R. W.; Debord, J.; Schaaff, T. G.; Whetten, R. L. *Anal. Chem.* **1999**, *71*, 3703–3711.
(39) Kim, Y. G.; Garcia-Martinez, J. C.; Crooks, R. M. *Langmuir* **2005**, *21*, 5485–5491.
(40) Quinn, B. M.; Liljeroth, P.; Ruiz, V.; Laaksonen, T.; Kontturi, K. *J. Am. Chem. Soc.* **2003**, *125*, 6644–6645.
(41) Chen, S.; Ingram, R. S.; Hostetler, M. J.; Pietron, J. J.; Murray, R. W.; Schaaff, T. G.; Khoury, J. T.; Alvarez, M. M.; Whetten, R. L. *Science* **1998**, *280*, 2098–2101.
(42) Stiles, R. L.; Balasubramanian, R.; Feldberg, S. W.; Murray, R. W. *J. Am. Chem. Soc.* **2008**, *130*, 1856–1865.
(43) Sardar, R.; Beasley, C. A.; Murray, R. W. *Anal. Chem.* **2009**, *81*, 6960–6965.
(44) Sardar, R.; Beasley, C. A.; Murray, R. W. *J. Am. Chem. Soc.* **2010**, *132*, 2058–2063.
(45) Heaven, M. W.; Dass, A.; S. White, P. S.; Holt, K. M.; Murray, R. W. *J. Am. Chem. Soc.* **2008**, *130*, 3754–3755.
(46) Zhu, M.; Aikens, C. M.; Frederick J. Hollander, F. J.; Schatz, G. C.; Jin, R. *J. Am. Chem. Soc.* **2008**, *130*, 5883–5885.
(47) Qian, H.; Eckenhoff, W.; Zhu, Y.; Pintauer, T.; Jin, R. *J. Am. Chem. Soc.* **2010**, *132*, 8280–8281.
(48) Jadzinsky, P. D.; Calero, G.; Ackerson, C. J.; Bushnell, D. A.; Kornberg, R. D. *Science* **2007**, *318*, 430–433.
(49) Whetten, R. L.; Price, R. C. *Science* **2007**, *318*, 407–408.
(50) Akola, A.; Walter, M.; Whetten, R. L.; Häkkinen, H.; Grönbeck., H. *J. Am. Chem. Soc.* **2008**, *130*, 3756–3757.
(51) Lopez-Acevedo, O.; Akola, J.; Whetten, R. L.; Grönbeck, H.; Häkkinen, H. *J. Phys. Chem. C* **2009**, *113*, 5035–5038.
(52) Brust, M.; W., M.; Bethell, D.; Schiffrin, D. J.; Whyman, R. J. *J. Chem. Soc., Chem. Commun.* **1994**, 801–802.
(53) Hostetler, M. J.; Wingate, J. E.; Zhong, C. J.; Harris, J. E.; Vachet, R. W.; Clark, M. R.; Londono, J. D.; Green, S. J.; Stokes, J. J.; Wignall, G. D.; Glish, G. L.; Porter, M. D.; Evans, N. D.; Murray, R. W. *Langmuir* **1998**, *14*, 17–30.
(54) Terrill, R. H.; Postlethwaite, T. A.; Chen, C.-H.; Poon, C.-D.; Terzis, A.; Chen, A.; Hutchison, J. E.; Clark, M. R.; Wignall, G.; *J. Am. Chem. Soc.* **1995**, *117*, 12537–12548.
(55) Weare, W. W.; Reed, S. M.; Warner, M. G.; Hutchison, J. E. *J. Am. Chem. Soc.* **2000**, *122*, 12890–12891.
(56) Qian, H.; Zhu, Y.; Jin, R. *ACS Nano* **2009**, *3*, 3795.
(57) Qian, H.; Zhu, Y.; Anderson, U. N.; Jin, R. *J. Phys. Chem. A* **2009**, *113*, 4281–4284.
(58) Zhu, M.; Lanni, M.; Garg, N.; Bier, M. E.; Jin, R. *J. Am. Chem. Soc.* **2008**, *130*, 1138–1139.
(59) Dass, A. *J. Am. Chem. Soc.* **2009**, *131*, 11666–11667.
(60) Reilly, S. M.; Krick, T.; Dass, A. *J. Phys. Chem. C* **2010**, *114*, 741–745.
(61) Goulet, P. G. J; R. Bruce Lennox, R. B. *J. Am. Chem. Soc.* **2010**, *132*, 9582–9584.
(62) Jana, N. R.; Peng, X. *J. Am. Chem. Soc.* **2003**, *125*, 14280–14281.
(63) Zheng, N.; Fan, J.; Stucky, G. D. *J. Am. Chem. Soc.* **2006**, *128*, 6550–6551.
(64) Dharmaratna, A. C.; Krick, T.; Dass, A. *J. Am. Chem. Soc.* **2009**, *131*, 13604–13605.
(65) Zheng, H.; Smith, R. K.; Jun, Y,-W.; Kisielowski, C.; Dahmen, U.; Alivisatos, A. P. *Science* **2009**, *324*, 1309–1312.
(66) Sardar, R.; Shumaker-Parry, J., S. *Chem. Mater.* **2009**, *21*, 1167–1169.
(67) Shem, P. M.; Sardar, R.; Shumaker-Parry, J., S. *Langmuir* **2009**, *25*, 13279–13283.
(68) Polte, J.; Erler, R.; Thu, A. F.; Thunemann, A. F.; Sokolov, S.; Ahner, T. T.; Rademann. Emmerling, F.; Kraehnert, R. *ACS Nano* **2010**, *4*, 1076–1082.
(69) Polte, J.; Ahner, T. T.; Delissen, F.; Sokolov, S.; Emmerling, F.; Thunemann, A. F.; Kraehnert, R. *J. Am. Chem. Soc.* **2010**, *132*, 1096–1301.
(70) Chen, C. F.; Tzeng, S. D.; Chen, H. Y.; Lin, K. J.; Gwo, S. *J. Am. Chem. Soc.* **2008**, *130*, 824–826.
(71) Bain, C. D.; Troughton, E. B.; Tao, Y. T.; Evall, J.; Whitesides, G. M.; Nuzzo, R. G. *J. Am. Chem. Soc.* **1989**, *111*, 321–335.
(72) Wang, Z. L.; Harfenist, S. A.; Whetten, R. L.; Bentley, J.; Evans, N. D. *J. Phys. Chem. B* **1998**, *102*, 3068–3072.
(73) Woehrle, G. H.; Warner, M. G.; Hutchison, J. E. *Langmuir* **2004**, *20*, 5982–5988.
(74) Sardar, R.; Funston, A. M.; Mulvaney, P.; Murray, R. W. *Langmuir* **2009**, *25*, 13840–13851.
(75) Peng, X. G.; Wickham, J.; Alivisatos, P. A. *J. Am. Chem. Soc.* **1998**, *120*, 5343–5344.
(76) Murray, C. B.; Kagan, C. B.; Bawendi, M. G. *Annu. Rev. Mater. Sci.* **2000**, *30*, 545–610.
(77) Shields, S. P.; Richards, V. N.; Buhro, W. E. *Chem. Mater.* **2010**, *22*, 3212–3225.
(78) Wolfe, R. L.; Murray, R. W. *Anal. Chem.* **2006**, *78*, 1167–1173.
(79) Brown, H. C.; Kulkarni, S. U. *Inorg. Chem.* **1977**, *16*, 3090–3094.
(80) Brown, H. C.; Kim, S. C.; Krishnamurthy, S. *J. Org. Chem.* **1980**, *45*, 1–12.
(81) Hussain, I.; Graham, S.; Wang, Z.; Tan, B.; Sherrington, D. C.; Rannard, S. P.; Cooper, A. I.; Brust, M. *J. Am. Chem. Soc.* **2005**, *127*, 16398–16399.
(82) Lummen, N. K., T. *Nanotechnology* **2005**, *16*, 2870–2877.
(83) Badia, A.; Singh, S.; Demers, L.; Cuccia, L.; Brown, R.; Lennox, R. B. *Chem.—Eur. J.* **1996**, *2*, 359–363.
(84) Badia, A.; Cuccia, L.; Demers, L.; Morin, F.; Lennox, R. B. *J. Am. Chem. Soc.* **1997**, *119*, 2682–2692.